

Unravelling competing microscopic interactions at a phase boundary: a single crystal study of the metastable antiferromagnetic pyrochlore $\text{Yb}_2\text{Ge}_2\text{O}_7$

C. L. Sarkis,¹ J. G. Rau,^{2,3,*} L. D. Sanjeeva,⁴ M. Powell,⁴ J. Kolis,⁴ J. Marbey,⁵ S. Hill,⁵ J. A. Rodriguez-Rivera,^{6,7} H. S. Nair,⁸ M. J. P. Gingras,^{9,10} and K. A. Ross^{1,10,†}

¹Department of Physics, Colorado State University, 200 W. Lake St., Fort Collins, CO 80523-1875, USA

²Max-Planck-Institut für Physik komplexer Systeme, 01187 Dresden, Germany

³Department of Physics, University of Windsor, 401 Sunset Avenue, Windsor, Ontario, N9B 3P4, Canada

⁴Department of Chemistry, Clemson University, Hunter Chemistry Laboratory, Clemson, SC 29634, USA

⁵Department of Physics and National High Magnetic Field Laboratory,

Florida State University, 1800 East Paul Dirac Drive, Tallahassee, Florida 32310, USA

⁶NIST Center for Neutron Research, National Institute of Standards and Technology, Gaithersburg, Maryland 20899, USA

⁷Materials Science and Engineering, University of Maryland, College Park, Maryland 20742, USA

⁸Department of Physics, University of Texas El Paso, 500 W University Ave, El Paso, Texas 79902

⁹Department of Physics and Astronomy, University of Waterloo, Ontario, N2L 3G1, Canada

¹⁰Quantum Materials Program, Canadian Institute for Advanced Research, MaRS Centre,

West Tower 661 University Ave., Suite 505, Toronto, ON, M5G 1M1, Canada

(Dated: December 20, 2019)

We report inelastic neutron scattering measurements from our newly synthesized single crystals of the structurally metastable antiferromagnetic pyrochlore $\text{Yb}_2\text{Ge}_2\text{O}_7$. We determine the four symmetry-allowed nearest-neighbor anisotropic exchange parameters via fits to linear spin wave theory supplemented by fits of the high-temperature specific heat. The exchange parameters so-determined are strongly correlated to the values determined for the g -tensor components, as previously noted for the related Yb pyrochlore $\text{Yb}_2\text{Ti}_2\text{O}_7$. To address this issue, we directly determined the g -tensor from electron paramagnetic resonance of 1% Yb-doped $\text{Lu}_2\text{Ge}_2\text{O}_7$, thus enabling an unambiguous determination of the exchange parameters. Our results show that $\text{Yb}_2\text{Ge}_2\text{O}_7$ resides extremely close to the classical phase boundary between an antiferromagnetic Γ_5 phase and a splayed ferromagnet phase. By juxtaposing our results with recent ones on $\text{Yb}_2\text{Ti}_2\text{O}_7$, our work illustrates that the Yb pyrochlore oxides represent ideal systems for studying quantum magnets in close proximity to classical phase boundaries.

Introduction — Phase competition in correlated electron systems is intimately linked to their novel behavior, such as high T_c superconductivity [1], colossal magnetoresistance [2], and the formation of quantum spin liquids (QSLs) [3]. Such complex systems with competing, or frustrated, interactions exhibit rich phase diagrams with many phase boundaries in their parameter space as vividly illustrated by highly-frustrated magnetic (HFM) systems [4]. Near phase boundaries – regions of strongest competition – quantum fluctuations can play an important role in shifting the phase boundaries, reducing the average order parameter, or potentially even destabilizing the nearby classical order altogether to produce intrinsically quantum states such as QSLs or valence bond/plaquette order [5–9]. Finding materials that lie close to classical phase boundaries can thus provide invaluable insights into the effects of competing quantum many-body interactions and result in the discovery of new phenomena. If a material, or family of materials, is thought to exhibit this phase competition, it is essential to determine precisely the nature of microscopic interactions. Unfortunately, the orientational averaging from polycrystalline (powder) samples can obscure important features, such as details of the excitation spectra, that are needed to fully characterize such systems. The study of high-quality single-crystals is thus crucial. In this work, we take advantage of the new availability of single crystals of the Yb pyrochlore $\text{Yb}_2\text{Ge}_2\text{O}_7$ to determine its microscopic exchange interactions and show that the $\text{Yb}_2\text{M}_2\text{O}_7$ family of pyrochlore oxides are

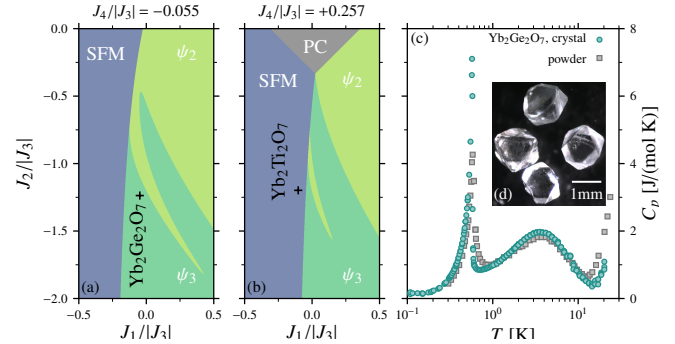


FIG. 1. (a,b) Sections of classical phase diagram for the anisotropic exchange model [Eq. (1)] relevant for (a) $\text{Yb}_2\text{Ge}_2\text{O}_7$ and (b) $\text{Yb}_2\text{Ti}_2\text{O}_7$. (c) Comparison of the specific heat of $\text{Yb}_2\text{Ge}_2\text{O}_7$ from a representative single crystal [10] and the powder sample studied in Ref. [11]. (d) Optical images of representative single crystals, adapted from Ref. [10].

exquisite materials for studying exotic phase boundary effects in HFM systems.

The rare-earth pyrochlore lattice materials beautifully exemplify the diversity of behaviors possible for competing interactions in frustrated effective spin- $\frac{1}{2}$ systems [12, 13]. At typical experimentally relevant temperature and energy scales, the angular momentum of the magnetic rare-earth ions can often be described as a pseudo-spin- $\frac{1}{2}$ with anisotropic effective

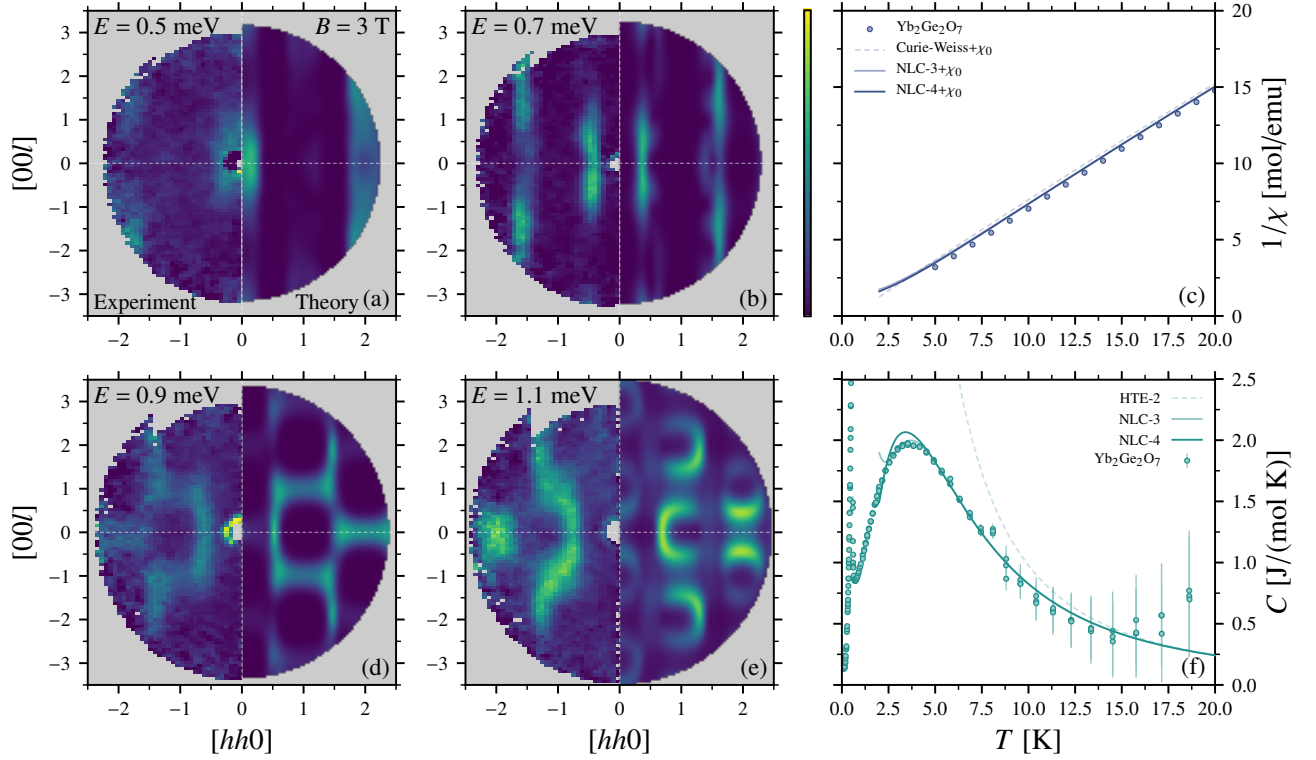


FIG. 2. (a,b,d,e) Comparison of constant-energy slices (centered at energy E with resolution $\Delta E = 0.17$ meV) of the 3 T field polarized spin-waves between $\text{Yb}_2\text{Ge}_2\text{O}_7$ at 1.8 K (left) and linear spin wave theory using the best fit J_1 - J_4 parameters within Eq. (1) (right). Comparison between the (c) magnetic susceptibility and (f) specific heat and NLC calculations for the parameters listed in Table I.

bilinear exchange interactions [13]. Detailed inelastic neutron scattering (INS) studies on single crystals of rare-earth titanate pyrochlores [14–17] have cemented the acceptance of a unifying minimal physical model [14, 15, 18] that underlies the behavior of many of these materials. This model is the nearest-neighbor (effective) spin- $\frac{1}{2}$ anisotropic exchange Hamiltonian for the pseudo-spins \mathbf{S} ,

$$H = \frac{1}{2} \sum_{\langle ij \rangle} \sum_{\mu\nu} J_{ij}^{\mu\nu} S_i^\mu S_j^\nu - \mu_B \sum_{\mu\nu} B^\mu \sum_i g_i^{\mu\nu} S_i^\nu, \quad (1)$$

where μ and ν run over the Cartesian directions (x, y, z), $J_{ij}^{\mu\nu}$ is the exchange tensor between spins at lattice sites i and j , $g_i^{\mu\nu}$ is the g -tensor for spin at site i , and B^μ is the μ component of the external magnetic field.

For the pyrochlore lattice, symmetry allows four independent exchange parameters (J_1, J_2, J_3, J_4) [14, 19]. As a function of these exchanges, the *classical* phase diagram contains four $q = 0$ ordered phases separated by several phase boundaries: three antiferromagnetic phases (the ψ_2 , ψ_3 and Palmer-Chalker, PC, states) and one splayed ferromagnet phase (SFM) [20, 21]. The Yb pyrochlore oxides $\text{Yb}_2\text{Ti}_2\text{O}_7$, $\text{Yb}_2\text{Ge}_2\text{O}_7$ and $\text{Yb}_2\text{Sn}_2\text{O}_7$ are prime candidates for realizing strong phase competition described by this model. While $\text{Yb}_2\text{Ge}_2\text{O}_7$ has been found to order into a Γ_5 AFM ground state (ψ_2 or ψ_3) [11], both $\text{Yb}_2\text{Ti}_2\text{O}_7$ [22–24] and $\text{Yb}_2\text{Sn}_2\text{O}_7$ [25, 26] order into SFM states. This strongly suggests that these three

materials lie close to a phase boundary between a Γ_5 phase and an SFM phase. To date, this has only been verified for $\text{Yb}_2\text{Ti}_2\text{O}_7$ [16, 17, 27, 28] due to the availability of large single crystals of that material.

In order to shed light on the evolution of this Yb series through the magnetic phase diagram, we have studied a collection of single crystals of $\text{Yb}_2\text{Ge}_2\text{O}_7$, which were recently successfully grown using a hydrothermal method [10], to determine the four exchange parameters of $\text{Yb}_2\text{Ge}_2\text{O}_7$. We find that the parameters for $\text{Yb}_2\text{Ge}_2\text{O}_7$ place it (classically) as close to the SFM/ Γ_5 phase boundary as $\text{Yb}_2\text{Ti}_2\text{O}_7$ is, but now *within* the Γ_5 phase, with the leading quantum fluctuations predicted to select a ψ_3 state, as we now proceed to show.

Material and methods — The cubic pyrochlore structure of $\text{Yb}_2\text{Ge}_2\text{O}_7$ (room temperature lattice parameter $a = 9.8297(7)\text{\AA}$ [10]) is a metastable phase. The thermodynamically stable crystal structure is the tetragonal pyrogermanate [10, 29–31], but the pyrochlore structure has been previously obtained as powder samples by high pressure and high temperature synthesis (1300°C, 6 GPa) [32, 33]. The growth of large single crystals that could readily be used for INS investigations is not yet possible under these extreme conditions, though $\text{Ho}_2\text{Ge}_2\text{O}_7$ and $\text{Dy}_2\text{Ge}_2\text{O}_7$ have been prepared very recently as small crystals under high pressure [34]. Meanwhile, a relatively low temperature hydrothermal synthesis (650°C) can stabilize the pyrochlore structure of $\text{Yb}_2\text{Ge}_2\text{O}_7$ and produce high quality single crystals of approximately $1 \times 1 \times 1$

mm³ size [10, 29]. Clear and colorless single crystals of cubic Yb₂Ge₂O₇ were prepared by this method [Figure 1(d)]. The temperature dependence of the specific heat, $C_p(T)$, measured on a 0.67 mg single crystal, was previously reported [10]; we reproduce it here for comparison to the powder data from Dun *et al.* [11, 35] [Figure 1(c)]. A broad feature centered around 3.5 K, and a sharp peak at $T_N = 0.572(4)$ K, are observed. Such features have been argued to correspond to the onset of short-range spin correlations and long-range order, respectively, in Yb pyrochlores [32, 36, 37]. The good agreement between the powder and the single crystal $C_p(T)$ data, the colorless appearance of the crystals, as well as the x-ray refinement results of Ref. [10], indicate that “stuffing” defects, or other non-idealities of the crystal structure that could produce a sample dependence of the physical properties [38–40], are negligible in our single crystals of Yb₂Ge₂O₇. Magnetic susceptibility data, $\chi(T)$, on the same single crystal (not oriented) were obtained using vibrating sample magnetometer from 100 K down to 1.8 K, in a field of 100 Oe. Electron paramagnetic resonance (EPR) spectra were recorded from a 50 mg collection of micro-crystals of 1% Yb doped Lu₂Ge₂O₇ (Lu_{1.98}Yb_{0.02}Ge₂O₇) which were synthesized in a similar manner as the Yb₂Ge₂O₇ crystals [10]. Several EPR spectra were taken at varying temperatures using a quasi-optical setup operating at 120 GHz [41]. Data at different temperatures were taken in order to observe that the resonance peak positions in the dilute compound do not shift, thus eliminating any possible concerns of spin interactions affecting the determination of the g -tensor.

INS data were collected using the Multi Axis Crystal Spectrometer (MACS) [42] at the NIST Center for Neutron Scattering, under an applied field up to 9 T. Twenty-eight single crystals of Yb₂Ge₂O₇ (total mass \sim 160 mg) were co-aligned on an oxygen-free copper mount to orient the $[hhl]$ plane horizontally and the field vertically along the $[1\bar{1}0]$ direction. The overall mosaic spread of the crystal array was found to be $\leq 5^\circ$ [43]. INS data were taken throughout the $[hhl]$ plane at a constant energy-transfer ($E = |E_f - E_i|$), using a fixed final energy of $E_f = 3.7$ meV and varying E_i , in a configuration [43] that produces an energy resolution of 0.17 meV at the elastic line. Although the sample was in a dilution refrigerator with base temperature of the mixing chamber reading 100 mK, comparison of our zero field base temperature data with data taken at 1.8 K suggests that the sample did not likely cool much below this higher temperature [43]. We therefore assign a temperature of our field-polarized INS measurements presented here to 1.8 K. This higher temperature does not affect the spin wave dispersions in the field-polarized paramagnetic state. Corresponding constant energy $[hhl]$ slices are shown in Fig. 2, where each energy slice took approximately 5 hours. The 3 T data, with 9 T data used as a background subtraction, was used in conjunction with thermodynamic and EPR data to determine the exchange parameters, as we describe below.

Results — First, we address the single-ion properties of Yb³⁺ in Yb₂Ge₂O₇. The site symmetry of Yb in the pyrochlore structure is trigonal (D_{3d}). This results in a g -tensor with two degenerate

Local	Global	Global (Alt.)	Dual (Alt.)
$J_{zz} = +0.1301$	$J_1 = -0.0175$	$J = -0.0175$	$\tilde{J} = +0.3414$
$J_{\pm} = +0.1358$	$J_2 = -0.4479$	$K = -0.4304$	$\tilde{K} = -0.0715$
$J_{\pm\pm} = +0.0365$	$J_3 = -0.3621$	$\Gamma = -0.3621$	$\tilde{\Gamma} = -0.0031$
$J_{z\pm} = -0.1903$	$J_4 = -0.0199$	$D = -0.0281$	$\tilde{D} = -0.2819$

TABLE I. Best fit exchange parameters (in meV) for Yb₂Ge₂O₇, determined from fitting INS and C_p , in several different (equivalent) presentations: local [15], global [14] and alternate global and dual global forms [47]

erate principal values in the local xy plane (g_{\pm}) and one unique value along the local z direction (g_z). Studies of Yb₂Ti₂O₇ have shown that the fitted g -tensor values determined via INS are strongly correlated with the determined exchange parameters when fitting field-polarized INS [17]. An unambiguous determination of the g -values, independent from the determination of the exchange parameters, is thus essential. Guided by this lesson, we used EPR to directly measure the g -tensor of 1% Yb doped Lu₂Ge₂O₇ on a randomly oriented collection of micro-crystals [44]. The spectrum shows an absorption range with limiting values corresponding to g -factors of $g_{\pm} = 4.20(5)$ and $g_z = 1.93(2)$ [43]. This confirms the xy anisotropy of the g -tensor in Yb₂Ge₂O₇, expected from powder studies [32], but does not agree quantitatively with previous determinations of the g -values from INS [32]. We attribute this disagreement to an intrinsic ambiguity in the fitting of the INS CEF data in Ref. [32], as we detail in the Supplemental Information [43].

With the single-ion properties determined, the exchange interactions (J_1, J_2, J_3, J_4) can next be obtained using the high-field spectrum. In a field of 3 T applied along $[1\bar{1}0]$, Yb₂Ge₂O₇ is in a field-polarized paramagnetic state and spin-wave excitations can be observed via INS. Due to the coarseness of the energy resolution of our measurement compared to the bandwidth, the dispersion of the excitations could not be reliably fit in the conventional way (as energy versus momentum relations) [43]. Therefore, to constrain the exchange interactions, we instead fit the intensity profile of the excitations in the $[hhl]$ plane at fixed energy-transfer (constant E), taking into account the energy resolution, as shown in Figure 2. The expected intensity was computed using the model Eq. (1) via linear spin-wave theory, with the g -tensor values fixed to those determined by EPR, [$g_{\pm} = 4.20(5)$ and $g_z = 1.93(2)$]. To further constrain the exchange parameters, we included in the fit the high-temperature part of the specific heat ($5 \text{ K} < T < 8 \text{ K}$) computed theoretically via a numerical linked-cluster expansion (NLC) [37, 43, 45, 46]. Our best fit exchange interactions are given in Table I, with Figure 2 showing the good agreement between the calculations and the data using the best-fit parameters.

Discussion — The determined exchange parameters place Yb₂Ge₂O₇ (Table I) very close to the (classical) boundary between the SFM and Γ_5 phases. They indicate that Yb₂Ge₂O₇ lies within the Γ_5 phase classically, with leading quantum

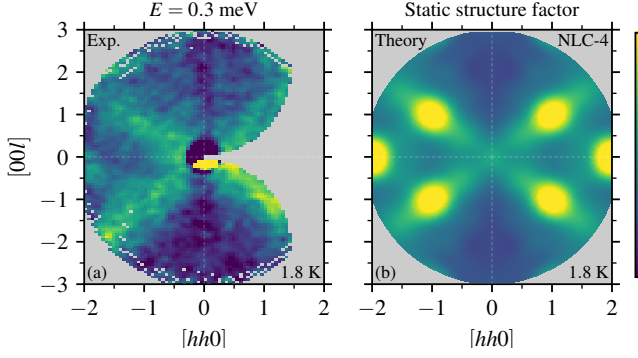


FIG. 3. (a) Constant energy transfer slice ($E = 0.3$ meV) for $\text{Yb}_2\text{Ge}_2\text{O}_7$ in zero field at $T = 1.8$ K. “Rods” of scattering are visible along $[111]$ directions as well as diffuse scattering at $[220]$. (b) Static (equal time) structure factor calculated using NLC at $T = 1.8$ K using our best fit parameters from the field-polarized spin waves (see Table I), which also shows rods of scattering and intensity at $[220]$

corrections selecting the ψ_3 state. This is consistent with the magnetic structure below T_N , which was previously reported to be either ψ_2 or ψ_3 [11]. While the classical phase boundaries of this model are known to shift due to quantum fluctuation effects [27, 48], typically the Γ_5 phase is expected to be *enlarged* due the presence of low-lying quasi-degenerate states [48]. We therefore do not expect quantum corrections to affect our assignment of $\text{Yb}_2\text{Ge}_2\text{O}_7$ to the Γ_5 phase. How the boundary between the ψ_2 and ψ_3 phases changes as one goes beyond the classical approximation is less clear. One might expect that the ψ_3 phase may be further stabilized at the expense of the ψ_2 phase due to additional soft modes that appear near the SFM phase boundary for the former [21, 49–51].

Our determination of the location of $\text{Yb}_2\text{Ge}_2\text{O}_7$ on the phase diagram confirms that changing the non-magnetic cation from Ti to Ge, which presumably alters the superexchange interactions by modifying distances and bond angles [47], is enough to push the Yb pyrochlores across the SFM- Γ_5 phase boundary. Yet, the titanate and germanate are otherwise extremely similar. The close relationship between these compounds is apparent even in powder samples; despite the disparate ordered ground states, a striking similarity is observed in the *powder averaged* zero field excitation spectra of the Yb pyrochlores as probed by INS [36], with each material exhibiting a continuum of excitations. One exciting potential explanation for the continuum is that the ordered phases in the $\text{Yb}_2\text{M}_2\text{O}_7$ family are “proximate” to an exotic QSL brought on by the phase competition.

Several regions of the $J_1 - J_4$ pyrochlore phase space are strongly frustrated and can thus lead to the appearance of *classical* spin liquids [52–54], the most famous being spin ice [53]. Upon inclusion of quantum fluctuations, these classical spin liquids can give way to true QSL states, such as quantum spin ice [55–58], and perhaps other QSL phases [59] that are likely lurking in this phase diagram. Due to their higher degeneracy, quantum fluctuation effects [21, 48] are enhanced, and so classical phase boundaries such as the one relevant to the Yb

pyrochlores are a good starting point to search for this kind of physics. The effects of a nearby QSL in the Yb pyrochlores could manifest as unusual excitations such as the ones observed in powder samples [36], as has been proposed for the α - RuCl_3 Kitaev material [60, 61]. The nearby QSL phase may be accessible via the application of chemical or external pressure, or perhaps a combination of both [62], to the Yb pyrochlores.

Regarding the zero-field spin excitations of single crystal $\text{Yb}_2\text{Ge}_2\text{O}_7$ for temperatures below T_N , we cannot comment further since we were limited to $T = 1.8$ K for our INS dataset. However, $T = 1.8$ K is below the Schottky-like hump in the specific heat, a feature that correlates with the onset of significant structured paramagnetic scattering in $\text{Yb}_2\text{Ti}_2\text{O}_7$ [63, 64] and other Yb pyrochlores [12] (as well as some reports of other quantum coherent phenomenon [65, 66]). We find that quasi-elastic paramagnetic scattering in $\text{Yb}_2\text{Ge}_2\text{O}_7$ at 0 T and 1.8 K qualitatively matches that of $\text{Yb}_2\text{Ti}_2\text{O}_7$ in the same regime; “rods” of scattering are observed along the $\langle 111 \rangle$ directions [63, 64], with a broad peak near $[220]$ [Fig. 3(a)]. A similar pattern is reproduced in the theoretical static structure factor computed via NLC (Fig. 3(b) using our best fit parameters). An interesting subject for future study would be to investigate the excitations of $\text{Yb}_2\text{Ge}_2\text{O}_7$ single crystals below T_N , and compare to $\text{Yb}_2\text{Ti}_2\text{O}_7$.

In summary, we have presented single crystal neutron scattering data from $\text{Yb}_2\text{Ge}_2\text{O}_7$, the sister compound of the well-studied pyrochlore $\text{Yb}_2\text{Ti}_2\text{O}_7$. We have determined accurate values of the g -tensor of $\text{Yb}_2\text{Ge}_2\text{O}_7$, measured directly by EPR spectroscopy of 1% Yb-doped $\text{Lu}_2\text{Ge}_2\text{O}_7$. Fits to field-polarized INS data, in conjunction with thermodynamic data, have allowed for the determination of the four symmetry-allowed nearest neighbor anisotropic exchange parameters for $\text{Yb}_2\text{Ge}_2\text{O}_7$. These parameters place $\text{Yb}_2\text{Ge}_2\text{O}_7$ exquisitely close to the classical phase boundary between the SFM and Γ_5 phase, just inside the Γ_5 phase, with leading quantum effects selecting a ψ_3 ground state. The zero field paramagnetic scattering in $\text{Yb}_2\text{Ge}_2\text{O}_7$ shows the same qualitative features as $\text{Yb}_2\text{Ti}_2\text{O}_7$. Our work demonstrates the striking similarity between these two unconventional pyrochlores, and definitively locates $\text{Yb}_2\text{Ge}_2\text{O}_7$ on the nearest-neighbor anisotropic exchange phase diagram that has been so successful in describing a variety rare-earth pyrochlores. Having established that $\text{Yb}_2\text{Ge}_2\text{O}_7$ resides close to the SFM/ Γ_5 boundary, and perhaps also close to the ψ_2/ψ_3 one [see Fig. 1(a)], one may now begin investigating how this affects the zero-field collective excitations of this compound [36]. Moreover, our work opens the door to future studies which aim to tune these Yb pyrochlores directly to the phase boundary, either by using pressure [62] or diluting the magnetic Yb sites as was done for $\text{Er}_{2-x}\text{Y}_x\text{Ti}_2\text{O}_7$ [67]. Finally, we have shown that relatively small single crystal samples obtained by hydrothermal synthesis can be used for detailed INS measurements, opening the door for other such measurements on crystals that can be grown using similar methods.

This research was partially supported by the CIFAR Quantum Materials program. KAR and CLS acknowledge support

from the Department of Energy award [de-sc0020071](#) during the preparation of this manuscript. Access to MACS was provided by the Center for High Resolution Neutron Scattering, a partnership between the National Institute of Standards and Technology and the National Science Foundation under Agreement No. DMR-1508249. This work was in part supported by Deutsche Forschungsgemeinschaft (DFG) under grant SFB 1143 and through the Würzburg-Dresden Cluster of Excellence on Complexity and Topology in Quantum Matter – *ct.qmat* (EXC 2147, project-id 39085490). The work at the University of Waterloo was supported by the Canada Research Chair program (M.J.P.G., Tier 1).

* jrau@uwindsor.ca

† Kate.Ross@colostate.edu

- [1] G. Grissonnache, O. Cyr-Choinière, F. Laliberté, S. R. De Cotret, A. Juneau-Fecteau, S. Dufour-Beauséjour, M.-E. Delage, D. LeBoeuf, J. Chang, B. J. Ramshaw, *et al.*, *Nature Communications* **5**, 3280 (2014).
- [2] E. Dagotto, *Science* **309**, 257 (2005).
- [3] L. Savary and L. Balents, *Reports on Progress in Physics* **80**, 016502 (2016).
- [4] C. Lacroix, P. Mendels, and F. Mila, *Introduction to Frustrated Magnetism* (Springer-Verlag, Berlin, Heidelberg, 2011).
- [5] P. Chandra and B. Doucot, *Physical Review B* **38**, 9335 (1988).
- [6] L. Capriotti and S. Sorella, *Physical Review Letters* **84**, 3173 (2000).
- [7] D. C. Cabra, C. A. Lamas, and H. D. Rosales, *Physical Review B* **83**, 094506 (2011).
- [8] J. Reuther, D. A. Abanin, and R. Thomale, *Physical Review B* **84**, 014417 (2011).
- [9] S.-S. Gong, W. Zhu, and D. N. Sheng, *Physical Review B* **92**, 195110 (2015).
- [10] L. D. Sanjeeva, K. A. Ross, C. L. Sarkis, H. S. Nair, C. D. McMillen, and J. W. Kolis, *Inorganic Chemistry* **57**, 12456 (2018).
- [11] Z. L. Dun, X. Li, R. S. Freitas, E. Arrighi, C. R. Delacruz, M. Lee, E. S. Choi, H. B. Cao, H. J. Silverstein, C. R. Wiebe, J. G. Cheng, H. D. Zhou *Physical Review B* **92**, 140407(R) (2015).
- [12] A. M. Hallas, J. Gaudet, and B. D. Gaulin, *Annual Review of Condensed Matter Physics* **9**, 105 (2018).
- [13] J. G. Rau and M. J. P. Gingras, *Annual Review of Condensed Matter Physics* **10**, 357 (2019).
- [14] K. A. Ross, L. Savary, B. D. Gaulin, and L. Balents, *Physical Review X* **1**, 021002 (2011).
- [15] L. Savary, K. A. Ross, B. D. Gaulin, J. P. C. Ruff, and L. Balents, *Physical Review Letters* **109**, 167201 (2012).
- [16] J. Robert, E. Lhotel, G. Remenyi, S. Sahling, I. Mirebeau, C. Decorse, B. Canals, and S. Petit, *Physical Review B* **92**, 064425 (2015).
- [17] J. D. Thompson, P. A. McClarty, D. Prabhakaran, I. Cabrera, T. Guidi, and R. Coldea, *Physical Review Letters* **119**, 057203 (2017).
- [18] M. E. Zhitomirsky, M. V. Gvozdikova, P. C. W. Holdsworth, and R. Moessner, *Physical Review Letters* **109**, 077204 (2012).
- [19] S. H. Curnoe, *Physical Review B* **78**, 094418 (2008).
- [20] A. W. C. Wong, Z. Hao, and M. J. P. Gingras, *Phys. Rev. B* **88**, 144402 (2013).
- [21] H. Yan, O. Benton, L. Jaubert, and N. Shannon, *Physical Review B* **95**, 094422 (2017).
- [22] Y. Yasui, M. Soda, S. Iikubo, M. Ito, M. Sato, N. Hamaguchi, T. Matsushita, N. Wada, T. Takeuchi, N. Aso, *et al.*, *Journal of the Physical Society of Japan* **72**, 3014 (2003).
- [23] J. Gaudet, K. A. Ross, E. Kermarrec, N. P. Butch, G. Ehlers, H. A. Dabkowska, and B. D. Gaulin, *Physical Review B* **93**, 064406 (2016).
- [24] A. Yaouanc, P. D. de Réotier, L. Keller, B. Roessli, and A. Forget, *Journal of Physics: Condensed Matter* **28**, 426002 (2016).
- [25] A. Yaouanc, P. Dalmasde Réotier, P. Bonville, J. A. Hodges, V. Glazkov, L. Keller, V. Sikolenko, M. Bartkowiak, A. Amato, C. Baines, P. J. C. King, P. C. M. Gubbens, A. Forget, *Physical Review Letters* **110**, 127207 (2013).
- [26] J. Lago, I. Živković, J. O. Piatek, P. Álvarez, D. Hübner, F. L. Pratt, M. Díaz, and T. Rojo, *Physical Review B* **89**, 024421 (2014).
- [27] J. G. Rau, R. Moessner, and P. A. McClarty, *Physical Review B* **100**, 104423 (2019).
- [28] A. Scheie, J. Kindervater, S. Zhang, H. Changlani, G. Sala, G. Ehlers, A. Heinemann, G. Tucker, S. Koohpayeh, and C. Broholm, *arXiv preprint [arXiv:1912.04913](#)* (2019).
- [29] L. N. Dem'yanets, S. F. Radaev, B. F. Mamin, and B. A. Maksimov, *Journal of Structural Chemistry* **29**, 485 (1988).
- [30] U. W. Becker and J. Felsche, *Journal of the Less Common Metals* **128**, 269 (1987).
- [31] L. Cai, A. L. Arias, and J. C. Nino, *Journal of Materials Chemistry* **21**, 3611 (2011).
- [32] A. M. Hallas, J. Gaudet, M. N. Wilson, T. J. Munsie, A. A. Aczel, M. B. Stone, R. S. Freitas, A. M. Arevalo-Lopez, J. P. Attfield, M. Tachibana, *et al.*, *Physical Review B* **93**, 104405 (2016).
- [33] R. D. Shannon and A. W. Sleight, *Inorganic Chemistry* **7**, 1649 (1968).
- [34] M. Antlauf, T. Taniguchi, J. Wagler, M. R. Schwarz, and E. Kroke, *Crystal Growth & Design* (2019).
- [35] Z. L. Dun, M. Lee, E. S. Choi, A. M. Hallas, C. R. Wiebe, J. S. Gardner, E. Arrighi, R. S. Freitas, A. M. Arevalo-Lopez, J. P. Attfield, *et al.*, *Physical Review B* **89**, 064401 (2014).
- [36] A. M. Hallas, J. Gaudet, N. P. Butch, M. Tachibana, R. S. Freitas, G. M. Luke, C. R. Wiebe, and B. D. Gaulin, *Physical Review B* **93**, 100403(R) (2016).
- [37] R. Applegate, N. R. Hayre, R. R. P. Singh, T. Lin, A. G. R. Day, and M. J. P. Gingras, *Physical Review Letters* **109**, 097205 (2012).
- [38] K. A. Ross, T. Proffen, H. A. Dabkowska, J. A. Quilliam, L. R. Yaraskavitch, J. B. Kycia, and B. D. Gaulin, *Physical Review B* **86**, 174424 (2012).
- [39] G. Sala, M. J. Gutmann, D. Prabhakaran, D. Pomaranski, C. Mitchelitis, J. B. Kycia, D. G. Porter, C. Castelnovo, and J. P. Goff, *Nature Materials* **13**, 488 (2014).
- [40] K. E. Arpino, B. A. Trump, A. O. Scheie, T. M. McQueen, and S. M. Koohpayeh, *Physical Review B* **95**, 094407 (2017).
- [41] J. Van Tol, L.-C. Brunel, and R. J. Wylde, *Review of Scientific Instruments* **76**, 074101 (2005).
- [42] J. A. Rodriguez, D. M. Adler, P. C. Brand, C. Broholm, J. C. Cook, C. Brocker, R. Hammond, Z. Huang, P. Hundertmark, J. W. Lynn, *et al.*, *Measurement Science and Technology* **19**, 034023 (2008).
- [43] “See supplemental material at [url will be inserted by publisher] for [give brief description of material].”
- [44] This collection of relatively large (compared to powder samples) crystals represents a large sampling of random orientations, but does not exactly correspond to a powder average. We did not pulverize the crystals in order to avoid strain broadening of the g-tensor.

- [45] B. Tang, E. Khatami, and M. Rigol, *Computer Physics Communications* **184**, 557 (2013).
- [46] N. R. Hayre, K. A. Ross, R. Applegate, T. Lin, R. R. P. Singh, B. D. Gaulin, and M. J. P. Gingras, *Physical Review B* **87**, 184423 (2013), 1211.5934.
- [47] J. G. Rau and M. J. P. Gingras, *Phys. Rev. B* **98**, 054408 (2018).
- [48] L. D. C. Jaubert, O. Benton, J. G. Rau, J. Oitmaa, R. R. P. Singh, N. Shannon, and M. J. P. Gingras, *Phys. Rev. Lett.* **115**, 267208 (2015).
- [49] M. Elhajal, B. Canals, R. Sunyer, and C. Lacroix, *Phys. Rev. B* **71**, 094420 (2005).
- [50] B. Canals, M. Elhajal, and C. Lacroix, *Phys. Rev. B* **78**, 214431 (2008).
- [51] G.-W. Chern, arXiv preprint [arXiv:1008.3038](https://arxiv.org/abs/1008.3038) (2010).
- [52] M. J. Harris, S. T. Bramwell, D. F. McMorrow, T. H. Zeiske, and K. W. Godfrey, *Physical Review Letters* **79**, 2554 (1997).
- [53] S. T. Bramwell and M. J. P. Gingras, *Science* **294**, 1495 (2001).
- [54] O. Benton, L. D. C. Jaubert, H. Yan, and N. Shannon, *Nature Communications* **7**, 11572 (2016).
- [55] M. Hermele, M. P. A. Fisher, and L. Balents, *Physical Review B* **69**, 064404 (2004).
- [56] H. R. Molavian, M. J. P. Gingras, and B. Canals, *Phys. Rev. Lett.* **98**, 157204 (2007).
- [57] S. Onoda and Y. Tanaka, *Phys. Rev. Lett.* **105**, 047201 (2010).
- [58] M. J. P. Gingras and P. A. McClarty, *Reports on Progress in Physics* **77**, 056501 (2014).
- [59] C. Liu, G. B. Halász, and L. Balents, *Physical Review B* **100**, 075125 (2019).
- [60] A. Banerjee, C. A. Bridges, J.-Q. Yan, A. A. Aczel, L. Li, M. B. Stone, G. E. Granroth, M. D. Lumsden, Y. Yiu, J. Knolle, *et al.*, *Nature materials* **15**, 733 (2016).
- [61] A. Banerjee, J. Yan, J. Knolle, C. A. Bridges, M. B. Stone, M. D. Lumsden, D. G. Mandrus, D. A. Tennant, R. Moessner, and S. E. Nagler, *Science* **356**, 1055 (2017).
- [62] E. Kermarrec, J. Gaudet, K. Fritsch, R. Khasanov, Z. Guguchia, C. Ritter, K. A. Ross, H. A. Dabkowska, and B. D. Gaulin, *Nature Communications* **8**, 14810 (2017).
- [63] K. A. Ross, J. P. C. Ruff, C. P. Adams, J. S. Gardner, H. A. Dabkowska, Y. Qiu, J. R. D. Copley, and B. D. Gaulin, *Phys. Rev. Lett.* **103**, 227202 (2009).
- [64] J. D. Thompson, P. A. McClarty, H. M. Rønnow, L. P. Regnault, A. Sørge, and M. J. P. Gingras, *Phys. Rev. Lett.* **106**, 187202 (2011).
- [65] Y. Tokiwa, T. Yamashita, M. Udagawa, S. Kittaka, T. Sakakibara, D. Terazawa, Y. Shimoyama, T. Terashima, Y. Yasui, T. Shibauchi, *et al.*, *Nature Communications* **7**, 10807 (2016).
- [66] L. Pan, N. J. Laurita, K. A. Ross, B. D. Gaulin, and N. P. Armitage, *Nature Physics* **12**, 361 (2016).
- [67] J. Gaudet, A. M. Hallas, D. D. Maharaj, C. R. C. Buhariwalla, E. Kermarrec, N. P. Butch, T. J. S. Munsie, H. A. Dabkowska, G. M. Luke, and B. D. Gaulin, *Phys. Rev. B* **94**, 060407(R) (2016).

**Supplemental Information for “Unravelling competing microscopic
interactions at a phase boundary:
a single crystal study of the metastable antiferromagnetic pyrochlore
 $\text{Yb}_2\text{Ge}_2\text{O}_7$ ”**

C. L. Sarkis,¹ J. G. Rau,^{2,3,*} L. D. Sanjeewa,⁴ M. Powell,⁴ J. Kolis,⁴ J. Marbey,⁵ S. Hill,⁵ J. A. Rodriguez-Rivera,^{6,7} H. S. Nair,⁸ M. J. P. Gingras,^{9,10} and K. A. Ross^{1,10,†}

¹*Department of Physics, Colorado State University,
200 W. Lake St., Fort Collins, CO 80523-1875, USA*

²*Max-Planck-Institut für Physik komplexer Systeme, 01187 Dresden, Germany*

³*Department of Physics, University of Windsor,
401 Sunset Avenue, Windsor, Ontario, N9B 3P4, Canada*

⁴*Department of Chemistry, Clemson University,
Hunter Chemistry Laboratory, Clemson, SC 29634, USA*

⁵*Department of Physics and National High Magnetic Field Laboratory,
Florida State University, 1800 East Paul Dirac Drive, Tallahassee, Florida 32310, USA*

⁶*NIST Center for Neutron Research, National Institute of Standards and Technology,
Gaithersburg, Maryland 20899, USA*

⁷*Materials Science and Engineering, University of Maryland,
College Park, Maryland 20742, USA*

⁸*Department of Physics, University of Texas El Paso,
500 W University Ave, El Paso, Texas 79902*

⁹*Department of Physics and Astronomy,
University of Waterloo, Ontario, N2L 3G1, Canada*

¹⁰*Quantum Materials Program, Canadian Institute for Advanced Research,
MaRS Centre, West Tower 661 University Ave.,
Suite 505, Toronto, ON, M5G 1M1, Canada*

(Dated: December 20, 2019)

S1. MAGNETIZATION

Magnetization on a small single crystal ($m = 0.68$ mg) of $\text{Yb}_2\text{Ge}_2\text{O}_7$ was performed using vibrating sample magnetometry (VSM) on a Quantum Design Dynacool PPMS. Three separate measurements were performed such that the field was aligned with each of the high symmetry directions of the pyrochlore lattice ([111], [110], [001]). Correct orientation was checked prior to and after measurement to rule out sample movement during the measurements. Magnetization versus field curves show a nearly isotropic response at $T = 2$ K and 10 K [Figure S1(a,c)]. The data are nearly in agreement with the expectations for the single-ion using the g -tensor values extracted from EPR [Figure S1(d)]. We also note that the saturated moment at 2 K, $\mu \sim 1.6\mu_B$, agrees well with previous literature [1]. The small deviations from the single ion model are likely attributable to the effect of exchange interactions, which are not negligible even relative to the maximum field strength.

Lower temperature (0.4 K) magnetization data with the field applied along [110] were collected using a Quantum Design MPMS SQUID magnetometer with ^3He insert [Figure S1(b)]. The data reveal a phase transition into the field-polarized paramagnetic state around 0.4 T.

S2. DETAILS OF INS MEASUREMENTS

Due to the difficulty in growing large (i.e., cm^3 sized) single crystals of the metastable pyrochlore phase of $\text{Yb}_2\text{Ge}_2\text{O}_7$, we were restricted to small high-quality single crystals (1mm x 1mm x 1mm). To increase the sample volume for neutron scattering, we co-aligned 28 small single crystals in the HHL scattering plane ([1 $\bar{1}$ 0] direction vertical) for a total mass of 154 mg [Figure S2(a)]. The crystals were fixed in place using a fluorinated glue (CYTOP 807-M). A rocking scan was taken over a [111] nuclear peak, shown in Figure S2(b). We note a peak splitting consistent with a mosaic of $\leq 5^\circ$ over all 28 crystals.

INS data were taken throughout the $[hhl]$ plane at a constant energy transfer ($E = |E_f - E_i|$), using a fixed final energy of $E_f = 3.7$ meV and varying E_i . The monochromator was used in doubly-focused mode with no radial collimators or filters in the incident beam, and cooled BeO filters were used in the scattered beam before the detectors. This configuration produces an energy

*Electronic address: jrau@uwindsor.ca

†Electronic address: Kate.Ross@colostate.edu

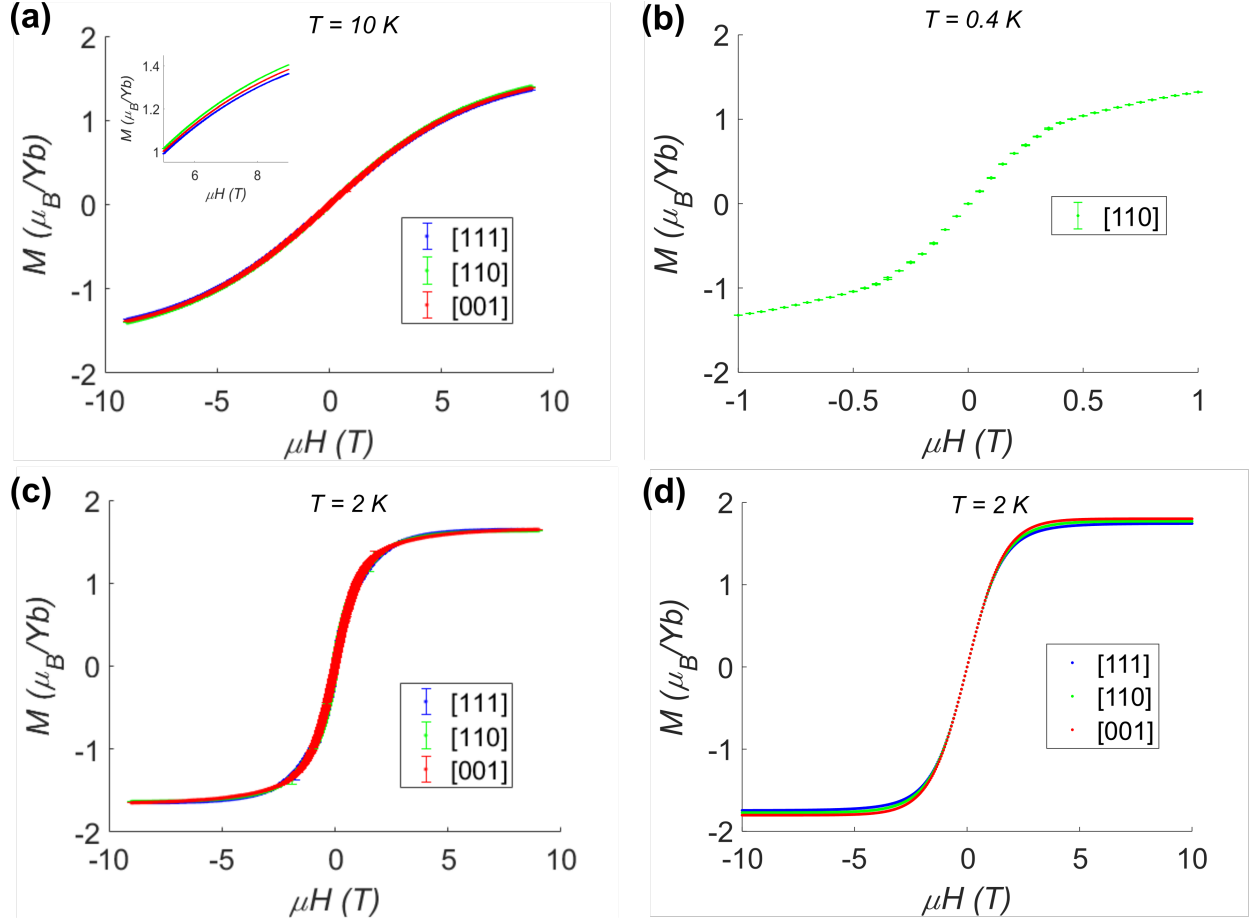


FIG. S1: Magnetization vs magnetic field for a $\text{Yb}_2\text{Ge}_2\text{O}_7$ single crystal. (a) Data taken at $T = 10\text{ K}$ for three high symmetry directions of pyrochlore lattice. (b) Data taken at $T = 0.4\text{ K}$, with field along [110]. (c) Data taken at $T = 2\text{ K}$. (d) Calculated single ion magnetization (using $g_z = 1.93$, $g_{\pm} = 4.20$) at $T = 2\text{ K}$.

resolution of 0.17 meV at the elastic line [2]. At each E (which increased in 0.1 meV steps from 0 to 1.5 meV), the sample was rotated through 180° in 2° increments, counting for 1.66×10^5 monitor units (approximately 10 s) at each increment.

As mentioned in the main text, data taken in zero field at the base temperature of the dilution refrigerator (mixing chamber temperature reading 260 mK) during the INS measurement is indistinguishable from data taken at 1.8 K . One possibility is that the inelastic spectrum is basically insensitive to temperature below 1.8 K , which would be largely consistent with a previous powder study [3]. However, in our experiment the elastic scattering also does not show any dependence on temperature below $T = 1.8\text{ K}$, even though it is clear that AFM Bragg peaks should develop below T_N (as has indeed been observed in the powder samples[1]). We can thus only conclude that the sample did not cool below T_N , potentially due to the large mass of the sample holder, or

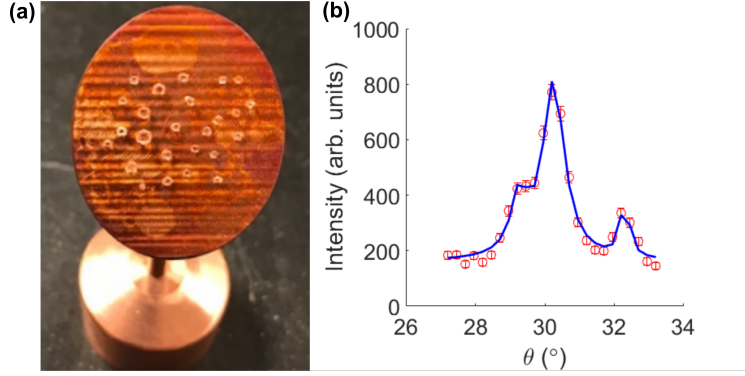


FIG. S2: (a): MACS neutron sample mount with 28 co-aligned single crystals of $\text{Yb}_2\text{Ge}_2\text{O}_7$. (b): Example rocking scan taken at MACS across a $[111]$ nuclear peak at $T \sim 6$ K. The peak is split into three peaks indicating a mosaic of $\leq 5^\circ$

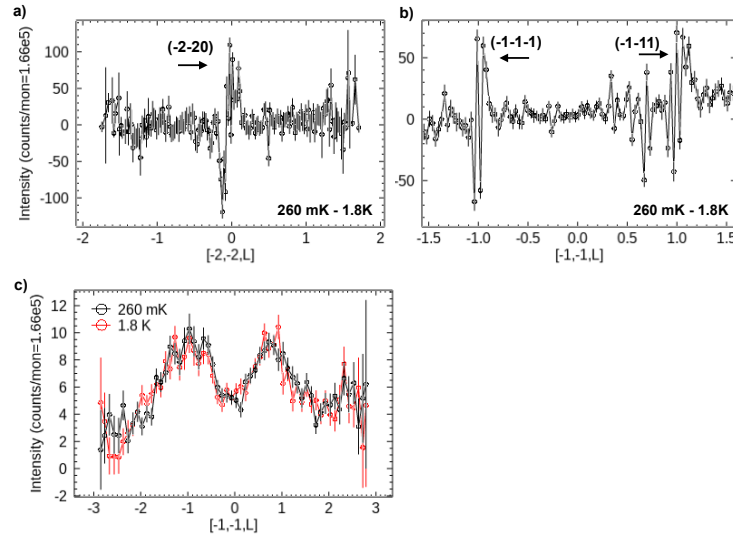


FIG. S3: Nominal temperature dependence of scattering. (a) and (b) show a lack of additional intensity on expected AFM Bragg peak positions. A shift of the peaks is observed instead (resulting in a net-zero profile with some regions of negative and positive differences). (c) overlay of the intensity along $[-1, -1, L]$ of the low energy excitations, $E = 0.3$ meV, at both temperatures (3 T data used as background subtraction).

weak thermal coupling between the small crystals and the sample holder. We thus assign a sample temperature of 1.8 K for our field-polarized INS data.

Figure S3 shows the comparison between the $T = 260$ mK (nominal) and $T = 1.8$ K data.

S3. DISPERSION OF 3 T DATA

Figure S4 shows INS data presented as a typical spin wave dispersion plot, illustrating that the energy resolution is insufficient to fit the dispersions themselves. Instead, we fit the intensity at several energies over the whole $[hhl]$ plane.

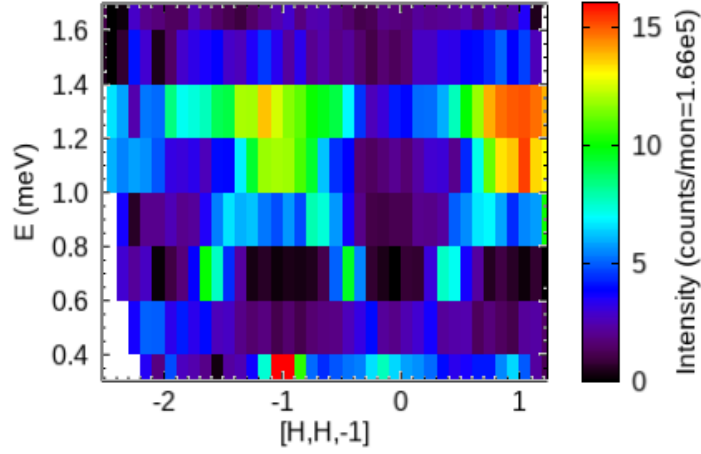


FIG. S4: $\text{Yb}_2\text{Ge}_2\text{O}_7$ INS data presented as a typical spin wave dispersion plot along $[H, H, -1]$. The dispersion is constructed from the combination of several constant energy slices through the $[hhl]$ plane.

S4. DETAILS OF FITTING

A. Ambiguities in fitting crystal field parameters

In this section, we address in more detail why it was necessary to obtain additional information above and beyond the inelastic neutron scattering data, specifically EPR on a diluted sample (as described in Sec. S5), to determine the g -factors.

A commonly used and reliable approach to finding the g -factors in a rare-earth magnet, such as $\text{Yb}_2\text{Ge}_2\text{O}_7$, is through determination of the parameters that describe the crystal field potential via fitting to experimental data. Typically, in INS measurements, the data used would be the transition energies and intensities between different crystal field multiplets. However, two issues present themselves in $\text{Yb}_2\text{Ge}_2\text{O}_7$. First, the energy scale of the crystal field is very large, with the gap between the ground and first excited doublet being ~ 80 meV [4]. At accessible experimental temperatures, one can thus only probe transitions from the ground doublet (which is essentially

fully populated) to the excited doublets (which are unpopulated). Second, for the D_{3d} environment of Yb^{3+} in $\text{Yb}_2\text{Ge}_2\text{O}_7$, the $J = 7/2$ manifold is split into only four Kramers doublets. Given the overall absolute intensity scale is (typically) difficult to determine, this leaves only *five* pieces of information: three transition energies (ground to excited levels for the reason stated above) and two relative transition intensities. This is less than the *six* parameters needed to describe the crystal field; usually denoted B_{20} , B_{40} , B_{60} , B_{43} , B_{63} and B_{66} (see, e.g. Ref. [5] for details). Such fitting, for example as carried out in Ref. [6] for $\text{Yb}_2\text{Ti}_2\text{O}_7$ and in Ref. [4] for $\text{Yb}_2\text{Ge}_2\text{O}_7$, is thus underconstrained and generically cannot yield a unique best fit. We note that in some ytterbium magnets where the crystal field energy scale is smaller, neutron data at several different temperatures may be used to resolve this issue (see, for example, Ref. [7]).

To make this point explicit, we have performed a re-analysis of the fitting results of Ref. [4] to highlight the non-uniqueness of the fit. Due to some ambiguities due to a phonon subtraction near the crystal field levels, we do *not* attempt to directly refit their intensity as a function of energy. Instead, we determine sets of crystal field parameters that can reproduce the best fit transition energies (ground to excited) and relative intensities (which can be calculated using the best fit CEF parameters of Ref. [4]), to within 1% accuracy. The result of this fitting is shown in Fig. S5, where one sees that a large number of crystal field parameters can produce nearly identical transitions and relative intensities as their best fit, but with wildly different g -factors. Indeed, the manifold of fits shown in Fig. S5 is (piece-wise) one-dimensional, as one would expect when trying to fit six parameters with only five pieces of data. One thus cannot use inelastic neutron scattering data alone to determine the g -factors in $\text{Yb}_2\text{Ge}_2\text{O}_7$.

We stress here that the set of g -factors in Fig. S5 does not exhaust all potential values of g_z and g_{\pm} relevant for $\text{Yb}_2\text{Ge}_2\text{O}_7$, since the phonon subtraction leaves a reasonable amount of uncertainty in properly assigning some of the transition energies and relative intensities. Indeed, our final g -factors, determined in the diluted sample via EPR (see Sec. S5), do not even show up in the manifold of fitted g parameters shown in Fig. S5.

We also explored a joint fit between the high temperature susceptibility and the crystal field data (three transitions and two relative intensities), as an alternative to the EPR from the diluted samples. These fits were inconclusive due to both the phonon subtraction issue discussed above, and some variability depending on the temperature range used in fitting the high-temperature susceptibility. We do note that, while not determinative, these results are somewhat consistent with the g -factors determined by EPR, i.e. $(g_z, g_{\pm}) = (1.93, 4.20)$. However, the Curie constant that was obtained by

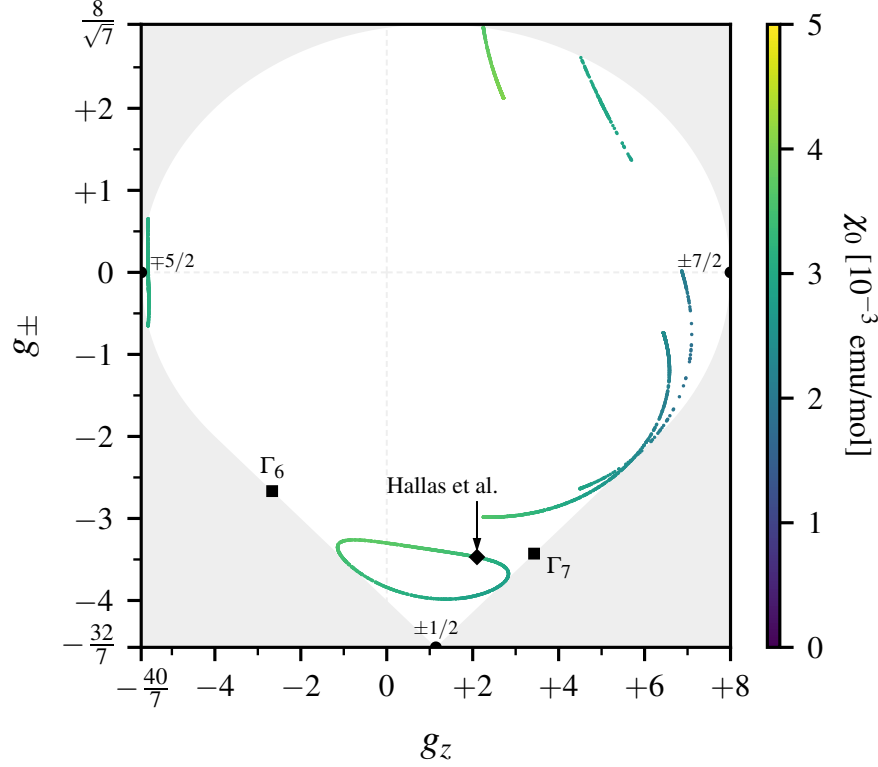


FIG. S5: Illustration of the non-uniqueness of the g -factors obtained from the fit reported in Ref. [4]. Each set of g -factors represents a set of six crystal field parameters (B_{kq}) with transition energies and relative intensities within 1% of the result computed using the best fit parameters of Ref. [4]. The color of each point show the variation of the Van Vleck contribution (χ_0) to the susceptibility. Several important limits are indicated: Γ_6 doublet (octahedron cage), Γ_7 doublet (cube cage), as well as pure $|\pm 1/2\rangle$, $|\pm 5/2\rangle$ and $|\pm 7/2\rangle$ doublets. The g -factors in the shaded region are not physical for a pure $J = 7/2$ manifold in a D_{3d} crystal field [8]

fitting the susceptibility was somewhat insensitive to the aforementioned confounding factors and is consistent with the EPR value.

B. Fitting of the exchange parameters

In this section, we describe our fitting methodology to determine the four exchange constants J_{zz} , J_{\pm} , $J_{\pm\pm}$ and $J_{z\pm}$ (or, equivalently, in the global or dual bases). Throughout, we fix the g -factors to the ones found from EPR, that is $(g_z, g_{\pm}) = (1.93, 4.20)$ (for details, see Sec. S5). We consider data

from two independent controlled “perturbative” regimes (high magnetic field or high temperature) to determine these four exchange constants.

First, is the inelastic response in the high-field partially polarized phase obtained by applying a $B = 3$ T magnetic field along $[1\bar{1}0]$ at $T = 1.8$ K. Theoretically, the inelastic response can be tractably calculated using standard linear spin-wave theory, as has been used in previous determinations of exchange constants in $\text{Yb}_2\text{Ti}_2\text{O}_7$ [9–11] and in $\text{Er}_2\text{Ti}_2\text{O}_7$ [12]. Due to experimental limitations (see Sec. S3), instead of fitting the spin-wave *spectrum*, we consider the inelastic intensity as a function of wave-vector (in the $[hhl]$ plane) within several fixed energy windows. Specifically, we consider the four energies $E = 0.5$ meV, 0.7 meV, 0.9 meV and 1.1 meV each averaged over an energy window with a resolution function characterized by a full width at half-maximum of 0.17 meV. To include the extent of the detectors out of the scattering plane, we also averaged over a window of $[-0.28, +0.28]$ r.l.u. in the $[1\bar{1}0]$ direction (the effect of finite resolution in the scattering plane is negligible for our purposes). The magnetic form factor of Yb^{3+} was included in the fitting [13], though the temperature is not, as the thermal population factors are unimportant even in the lowest energy window considered. Further, given we fit within (somewhat) narrow energy windows, any thermal factors primarily affect the overall intensity scale, not the variation with wave-vector.

Second, we make use of the specific heat data at zero field, but at high temperatures. This high temperature regime can be readily accessed using series expansion techniques. For this purpose, we employ a numerical linked-cluster expansion [14–16] to third order (NLC-3) in the number tetrahedra [17–19]. This order in the expansion is sufficient for good convergence in the temperature range considered for typical exchange constants, yet sufficiently fast computationally to still be amenable to automated fitting. More specifically, we consider five temperatures in the range $5 \text{ K} \leq T \leq 8 \text{ K}$ (to minimize any phonon effects) with the specific heat of the non-magnetic analogue $\text{Lu}_2\text{Ge}_2\text{O}_7$ subtracted [1].

For each comparison to experimental data (high-field inelastic response or high-temperature specific heat), we evaluate a χ^2 value using estimates of the experimental errors, then sum these to obtain a total χ^2 value. This total χ^2 is then minimized to find the best fit (via standard Nelder-Mead simplex method implementation). To ensure that we find the global minimum, we repeat the fitting procedure $O(10^2)$ times from random initial points, typically taking each of the four exchanges ($J_{zz}, J_{\pm}, J_{\pm\pm}, J_{z\pm}$) to be chosen independently and uniformly in the range -0.2 meV to $+0.2$ meV.

The best fit found is

$$J_{zz} = +0.1302 \text{ meV}, \quad J_{\pm} = +0.1358 \text{ meV}, \quad J_{\pm\pm} = +0.0365 \text{ meV}, \quad J_{z\pm} = -0.1903 \text{ meV}, \quad (\text{S1})$$

as given in Table I of the main text. We note that there was a local minimum with higher, but comparable χ^2 to the best fit presented here, with parameters $(J_{zz}, J_{\pm}, J_{\pm\pm}, J_{z\pm}) = (+0.1774, +0.1325, +0.0269, -0.1824) \text{ meV}$. This alternate parameter set has many of the same features of the best fit, such as a ψ_3 ground state and close proximity to the SFM phase boundary, differing mainly in its larger value for J_{zz} . Previous fits of experimental data in $\text{Yb}_2\text{Ti}_2\text{O}_7$ have also found J_{zz} to be constrained more loosely than the other fitted exchange parameters [11].

We note that we also attempted determining the g -factors without the EPR data, using only the high-field inelastic neutron scattering data and the Curie constant obtained from the magnetic susceptibility. Including the Curie constant fixes $\bar{g}^2 \equiv g_z^2 + 2g_{\pm}^2$, giving the pair of g -factors in terms of a single angle, θ , as $g_z = \bar{g} \cos \theta$ and $g_{\pm} = \bar{g} \sin \theta / \sqrt{2}$. The fitting procedure described above was then carried out on the high-field inelastic neutron scattering data alone, on a grid to determine the value of θ having the lowest χ^2 . This was inconclusive, given the issues described above with temperature range dependence in determining the Curie constant and a large number of nearly equally good local minima. However, we do note that the g -factor values obtained via the EPR measurements did appear among these local minima determined using susceptibility data.

S5. EPR DETERMINATION OF g -TENSOR

Continuous wave (CW) powder EPR experiments were performed using a superheterodyne quasi-optical spectrometer described in Ref. [20]. The measurements were performed on a coarse powder of micro-crystalline material (1% Yb^{3+} in $\text{Lu}_2\text{Ge}_2\text{O}_7$) to avoid any sample degradation that might result from over-grinding to the degree usually necessary for powder EPR studies. Because of this, many sharp, albeit weak resonances corresponding to individual randomly oriented micro-crystals can be observed in between the extremes of the spectra; these resonances give the appearance of an increased noise level, but they are real signals from individual micro-crystals. The sample was remeasured multiple times after stirring to confirm a re-distribution of the stronger signals. The principal components of the g -tensor, quoted in the main text, were determined from the end-points of the 120 GHz EPR absorption profile. These end-points manifest as a first derivative in the recorded spectrum (Figure S6) due to the use of field modulation and lock-in

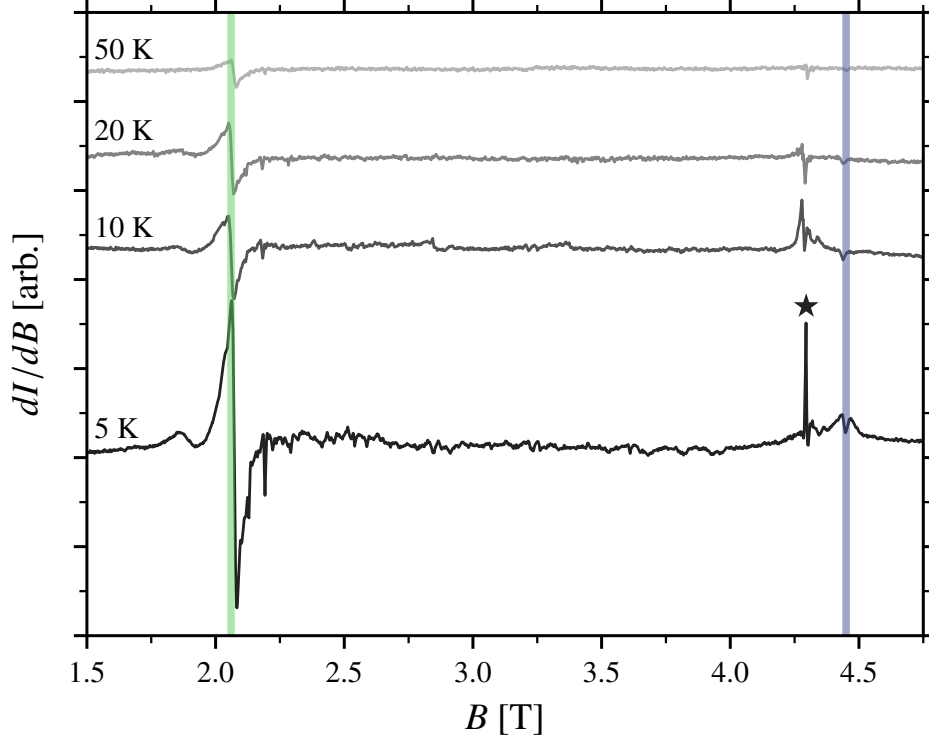


FIG. S6: EPR spectra from a 50mg collection of 1% Yb-doped $\text{Lu}_2\text{Ge}_2\text{O}_7$ microcrystallites at different temperatures (arbitrary scale, offset for clarity). The g -tensor values are determined from the minimum and maximum of the broad EPR absorption, $g_{\pm} = 4.20(5)$, $g_z = 1.93(2)$, which are shown with the green and blue vertical lines. An unidentified $g \approx 2$ impurity is present (indicated by the star).

detection of the in-phase signal. For an axial spectrum ($g_x = g_y \neq g_z$), as expected on the basis of the local site symmetry at the Yb sites, sharp features in the first derivative spectrum are expected only at the onset and cessation of the absorption profile, i.e., the end-points of the spectrum. For the easy-plane case ($g_x = g_y > g_z$), a biased spectral intensity with a derivative lineshape is expected on the low-field end of the spectrum (absorption onset), with a dip at the high-field end (cessation of the absorption). The low-field signal may be further biased in a loose powder due to torqueing and preferential alignment of individual microcrystals. Therefore, we associate the strong derivative signal centered just above 2.0 T (frequency = 120.0 GHz) with g_x and $g_y = 4.20(5)$. A weak dip corresponding to the g_z component of the spectrum is harder to pick-out, as it rides on top of a broad signal spanning the $g = 2.00$ region that we ascribe to paramagnetic contaminants; the sharp signal exactly at $g = 2.00$, marked with an asterisk in Fig. 3, is also assigned to an impurity. Nevertheless, the sharp dip at the $g_z = 1.93(2)$ position persists to high temperatures and is consistent with signals observed each time the sample was re-measured. Error bars were determined from the linewidths of

the observed signals (peak-to-peak linewidth in the case of the g_x/g_y signal). Finally, the fact that the resonance positions do not shift upon varying the temperature indicates that magnetic interactions do not influence the measurements, thus confirming that the EPR is in fact probing the isolated Yb sites in the diluted sample. By contrast, measurements performed on concentrated samples (100% Yb³⁺ in place of Lu³⁺) revealed broad EPR signals with strongly temperature dependent effective g -values, strongly shifted from the free-ion values due to the Yb-Yb exchange.

-
- [1] Z. L. Dun, X. Li, R. S. Freitas, E. Arrighi, C. R. D. Cruz, M. Lee, E. S. Choi, H. B. Cao, H. J. Silverstein, C. R. Wiebe, et al., *Physical Review B* **92**, 140407 (2015).
 - [2] *Mac's ii overview*, <https://www.ncnr.nist.gov/instruments/macs/Overview.html>, accessed: 2019-09-20.
 - [3] A. M. Hallas, J. Gaudet, N. P. Butch, M. Tachibana, R. S. Freitas, G. M. Luke, C. R. Wiebe, and B. D. Gaulin, *Physical Review B* **93**, 100403 (2016).
 - [4] A. M. Hallas, J. Gaudet, M. N. Wilson, T. J. Munsie, A. A. Aczel, M. B. Stone, R. S. Freitas, A. M. Arevalo-Lopez, J. P. Attfield, M. Tachibana, et al., *Physical Review B* **93**, 104405 (2016).
 - [5] A. Bertin, Y. Chapuis, P. D. de Réotier, and A. Yaouanc, *Journal of Physics: Condensed Matter* **24**, 256003 (2012).
 - [6] J. Gaudet, D. D. Maharaj, G. Sala, E. Kermarrec, K. A. Ross, H. A. Dabkowska, A. I. Kolesnikov, G. E. Granroth, and B. D. Gaulin, *Phys. Rev. B* **92**, 134420 (2015).
 - [7] G. Sala, M. Stone, B. K. Rai, A. F. May, D. S. Parker, G. B. Halász, Y. Q. Cheng, G. Ehlers, V. O. Garlea, Q. Zhang, et al., arXiv preprint [arXiv:1907.10627](https://arxiv.org/abs/1907.10627) (2019).
 - [8] J. G. Rau and M. J. P. Gingras, *Phys. Rev. B* **98**, 054408 (2018).
 - [9] K. A. Ross, L. Savary, B. D. Gaulin, and L. Balents, *Physical Review X* **1**, 021002 (2011).
 - [10] J. Robert, E. Lhotel, G. Remenyi, S. Sahling, I. Mirebeau, C. Decorse, B. Canals, and S. Petit, *Physical Review B* **92**, 064425 (2015).
 - [11] J. D. Thompson, P. A. McClarty, D. Prabhakaran, I. Cabrera, T. Guidi, and R. Coldea, *Physical Review Letters* **119**, 057203 (2017).
 - [12] L. Savary, K. A. Ross, B. D. Gaulin, J. P. C. Ruff, and L. Balents, *Physical Review Letters* **109**, 167201 (2012).
 - [13] P. Brown, *International Tables for Crystallography*, vol. C (Springer, 2006).

- [14] M. Rigol, T. Bryant, and R. R. P. Singh, Phys. Rev. Lett. **97**, 187202 (2006).
- [15] M. Rigol, T. Bryant, and R. R. P. Singh, Phys. Rev. E **75**, 061118 (2007).
- [16] B. Tang, E. Khatami, and M. Rigol, Computer Physics Communications **184**, 557 (2013).
- [17] N. R. Hayre, K. A. Ross, R. Applegate, T. Lin, B. D. Gaulin, R. R. P. Singh, and M. J. P. Gingras, Physical Review B. **87**, 184423 (2013), 1211.5934.
- [18] R. Applegate, N. R. Hayre, R. R. P. Singh, T. Lin, A. G. R. Day, and M. J. P. Gingras, Physical Review Letters **109**, 097205 (2012).
- [19] L. D. C. Jaubert, O. Benton, J. G. Rau, J. Oitmaa, R. R. P. Singh, N. Shannon, and M. J. P. Gingras, Phys. Rev. Lett. **115**, 267208 (2015).
- [20] J. Van Tol, L.-C. Brunel, and R. J. Wylde, Review of Scientific Instruments **76**, 074101 (2005).